

# Decreasing the non-linearity of hybrid reluctance actuators by air gap design

Alexander Pechhacker<sup>a</sup>, Ernst Csencsics<sup>a</sup>, Georg Schitter<sup>a</sup>

<sup>a</sup>Automation and Control Institute, TU Wien, Gußhausstraße 27-29, Vienna, 1040, Austria

## Abstract

This paper presents an air gap design approach to improve the linearity of rotational Hybrid Reluctance Actuators (HRAs) used in fast steering mirrors. The approach involves modeling a one-degree-of-freedom HRA with a magnetic equivalent circuit to identify and analyze sources of non-linearities. On the basis of the verified model, solutions for an improved linear system behavior are analytically searched. Two linearized HRA designs are proposed, one with linear cross-section dependency and the other with hyperbolic air gap length dependency. Finite element method simulations are employed to evaluate the performance with respect to the linearity and the motor constant of these designs, showing factor 50 improved system linearity.

**Keywords:** Actuators, Magnetics, Hybrid reluctance actuation (HRA), Linearization, Fast steering mirror, Magnetic equivalent circuit.

## 1. Introduction

The actuation technology significantly defines the performance of mechatronic systems, with respect to range and bandwidth. Mechatronic systems are commonly driven by piezo actuators for high bandwidth applications but limited range or Lorentz actuators for large range applications but limited bandwidth. In recent years hybrid reluctance actuators (HRAs) revealed the highest range-bandwidth product [1]. Furthermore, HRAs are shown to deliver higher forces per volume with higher motor constants than Lorentz actuators [2].

HRAs are used in a large number of applications, ranging from nanopositioning systems [3, 4, 5, 6] to linear scanners [7, 8], positioning systems with zero-power gravity compensation [9], deformable mirrors [10, 11], fast tool servos [12, 13, 14] and self-holding actuators for mechanical gear shifting [15].

HRAs are particularly widespread in fast steering mirrors [16, 17, 18, 19, 20, 21, 22, 23, 24, 25]. Fast steering mirrors are high performance optomechatronic systems, which can be distinguished based on their application into pointing and scanning. Pointing applications involve tasks such as stabilizing optical systems in optical free-space communication [26], acquisition of optical signals and tracking of objects [27] and pointing of laser or light beams on a target [28]. Scanning applications are even more extensive, including laser scanning [29], material processing [30], scanning optical lithography [31], confocal microscopy [32] and inline metrology [33]. All these applications desire an actuation technology, that is compact for system integration and efficient to avoid negative thermal impairment of the mirror surface or the nearby sensors. HRAs are a promising actuation technology with respect to those two key characteristics.

However, conventional HRAs have a non-linear system behaviour, causing a operating point-dependent performance and properties, such as the stiffness of the system and the motor

constant [20]. This system non-linearity might impair the system performance due to the following effects. First, the non-linear dynamics of the system significantly increases the design complexity of the control system by requiring non-linear feedback and/or feedforward compensators [4, 34, 35]. Second, unlike Lorentz-actuated systems with zero stiffness, which is a key property for vibration isolation and high-precision positioning systems, the variable negative stiffness of HRAs cannot be compensated independently of the operating point by mechanical flexures [36, 8]. Third, position-dependent resonance frequencies reduce the efficiency in resonant scanning applications [22, 5]. These drawbacks prevent the use of conventionally non-linear HRA technology in highly linear mechatronic systems. The need for electromagnetically actuated systems with linear dynamics can be observed by several examples, such as, linearization of magnetic bearings by non-linear feedforward or feedback compensators [37, 38, 39] and linearization by intelligent current, voltage and magnetic flux conditions [40].

This paper proposes a design approach to improve the linearity of rotational HRAs used in fast steering mirrors. By modeling a one-degree-of-freedom HRA with a magnetic equivalent circuit, the source of the non-linear system behaviour are identified and discussed in Section 2. On the basis of the evaluated magnetic equivalent circuit, solutions for an improved linear system behavior are analytically derived in Section 3. The solutions of the linearized HRAs, as well as the conventional HRA, are evaluated by finite element method (FEM) simulations and the resulting performance is discussed in Section 4.

## 2. Modeling of conventional hybrid reluctance actuators

State of the art HRAs demonstrate a non-linearity in the torque acting on the mover with respect to the angular deflection and the coil current. To identify the source of this undesired

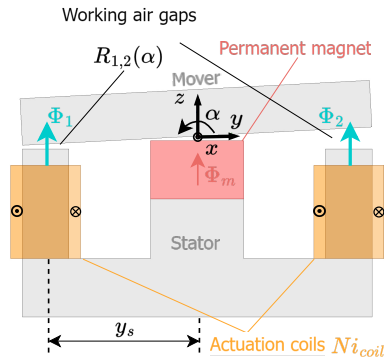


Figure 1: Conventional design of a titling HRA with a central permanent magnet indicated in red (NdFeB, Grade 45,  $8 \times 5 \times 5 \text{ mm}^3$ ), the ferromagnetic components in gray (Carbon Steel, Grade 1008), and the actuation coils in orange (number of turns  $N = 300$ ).

non-linearity, a one degree-of-freedom is HRA modeled. Due to the good compromise between complexity and accuracy, a magnetic equivalent circuit is used to model the rotational HRA [41]. Based on the magnetic equivalent circuit, the magnetic fluxes are obtained and the resulting, non-linearly depending torque acting on the mover can be determined.

Generally, HRAs consist of the following main components:

- One or multiple permanent magnets to introduce a biasing magnetic flux in the working air gaps,
- One or multiple actuation coils to dynamically adapt the magnetic flux in the working air gaps,
- A ferromagnetic mover
- A ferromagnetic stator to guide the magnetic flux in the non-moving part.

The literature reveals many different versions of HRA designs consisting of the main components mentioned [25, 20, 16, 19, 18]. This paper focuses on a design with one permanent magnet, an angular range of  $\pm 4^\circ$  (mechanical) and two actuation coils due to compactness and performance [20], shown in Fig. 1. However, the subsequently defined design guidelines to improve linearity can be applied to all HRA designs, which can be modelled with the subsequently derived magnetic equivalent circuit model, shown in Fig. 2.

The magneto motive forces (MMF) of the magnetic equivalent circuit are defined by

$$\begin{aligned}\Psi_1(i_{coil}) &= \frac{Ni_{coil}}{2} \\ \Psi_2(i_{coil}) &= -\frac{Ni_{coil}}{2} \\ \Psi_m &= H_c l_m\end{aligned}\quad (1)$$

with the MMF of the actuation coils  $\Psi_1, \Psi_2$ , the MMF due to the magnetization of the permanent magnet  $\Psi_m$ , the number of

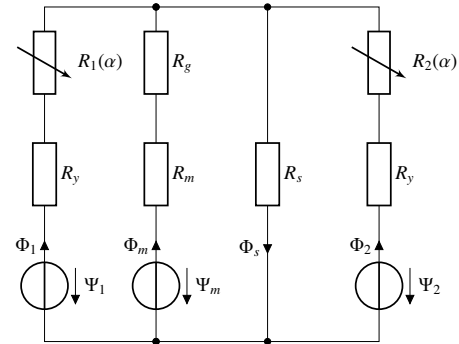


Figure 2: Magnetic equivalent circuit of a conventional HRA with the reluctances  $R$ , the magneto motive forces  $\Psi$  and the fluxes  $\Phi$ .

turns of both actuation coils  $N$  and the coil current  $i_{coil}$ . A constant MMF  $\Psi_m$  models the permanent magnet with the coercivity of the magnetic material  $H_c$  and the length of the permanent magnet  $l_m$ , which introduces a biasing magnetic flux in the working air gaps. The coil current  $i_{coil}$  in  $\Psi_1$  and  $\Psi_2$  is reversed to obtain increasing/decreasing magnetic fluxes in the working air gaps  $\Phi_1$  and  $\Phi_2$ , respectively. This principle enables bidirectional torques of rotational HRAs by two unidirectional reluctance forces in a pull/pull configuration [17].

The reluctances of the magnetic equivalent circuit model are defined by

$$\begin{aligned}R_1(\alpha) &= \frac{-\alpha y_s + x_0}{\mu_0 A} & R_2(\alpha) &= \frac{\alpha y_s + x_0}{\mu_0 A} \\ R_m &= \frac{l_m}{\mu_0 A_m} & R_g &= \frac{l_g}{\mu_0 A_m} \\ R_s &= \frac{l_s}{\mu_0 A_s} & R_y &= \frac{l_y}{\mu_0 \mu_y A_y}\end{aligned}\quad (2)$$

with the constant reluctances of the permanent magnet  $R_m$ , the non-working air gap above the permanent magnet  $R_g$  and a reluctance  $R_y$  to model the stator, as well as the mover yoke. Corresponding air gap lengths, cross-sections and permeabilities are denoted with  $l, A$  and  $\mu$ , respectively. The position-dependent reluctances, defined as  $R_1(\alpha)$  and  $R_2(\alpha)$ , describe the behavior of the left and right working air gap with  $x_0$  being the air gap length for  $\alpha = 0^\circ$ . Due to the limited range of  $\pm 4^\circ$  and the subsequent analytical discussion, the change of the air gap length between mover and stator in relation to the angular deflection  $\alpha$  is modeled using the small angle approximation  $y_s \sin \alpha \approx y_s \alpha$  with  $y_s$  being the distance from the axis of rotation ( $x$ -axis) to the center of the stator yoke. In addition to the desired main flux paths  $\Phi_1, \Phi_2$  and  $\Phi_m$ , a stray reluctance  $R_s$  is connected in parallel to model the stray flux  $\Phi_s$ . The stray reluctance models flux paths, which are not contributing to the mover torque, e.g. to the rotation axis radially oriented flux components or magnetic fluxes from the vertical surface of the permanent magnet to the stator.

By applying Gauss's and Ampere's law on the magnetic equivalent circuit in Fig. 2, the following circuit equations are

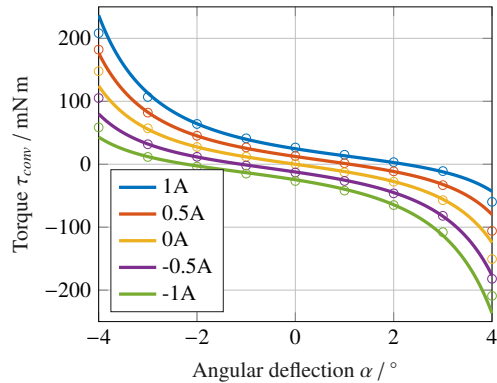


Figure 3: Mover torque of the conventional HRA. Comparison of the FEM simulations (circles) and the magnetic equivalent circuit (lines) at various coil currents  $i_{coil}$ , clearly indicating the non-linearity, especially towards increasing angular deflections.

derived

$$\begin{aligned}\Psi_1 &= \Phi_1 (R_1 + R_y) - \Phi_m (R_m + R_g) + \Psi_m \\ \Psi_2 &= \Phi_2 (R_2 + R_y) - \Phi_m (R_m + R_g) + \Psi_m \\ \Psi_m &= \Phi_m R_m + \Phi_s R_s \\ \Phi_s &= \Phi_1 + \Phi_2 + \Phi_m\end{aligned}\quad (3)$$

with the previously defined MMFs  $\Psi$ , magnetic fluxes  $\Phi$  and reluctances  $R$ . By eliminating  $\Phi_m$  and  $\Phi_s$  in Eq. (3), the magnetic fluxes in the working air gaps can be expressed with Eq. (1) and (2) as functions of the coil current and the angular deflection of the mover, denoted as  $\Phi_1(\alpha, i_{coil})$  and  $\Phi_2(\alpha, i_{coil})$ .

With the derived magnetic fluxes in the working air gaps between mover and stator, the torque acting on the mover is determined based on the reluctance force by [5] and the small angle approximation  $\cos \alpha \approx 1$

$$\tau_{conv}(\alpha, i_{coil}) = \frac{\Phi_1^2(\alpha, i_{coil}) - \Phi_2^2(\alpha, i_{coil})}{2\mu_0 A} y_s \quad (4)$$

with the permeability of vacuum  $\mu_0$ , the cross-section of the stator yoke at the air gap  $A$  and the distance from the axis of rotation (x-axis) to the center of the stator yoke  $y_s$ . Due to the alignment of the permanent magnet in the center and the symmetric design, the mover torques resulting from the magnet flux of the permanent magnet  $\Phi_m$  or the stray flux  $\Phi_s$  are negligible. In the remaining mover degrees of freedom, torques and forces are absorbed by an external structure, e.g. a flexure hinge or a bearing [42, 43].

For verification of the introduced magnetic equivalent circuit model, FEM simulations (Maxwell 3D, Ansys Inc., USA) with non-linear BH curves for the ferromagnetic parts (Carbon Steel, Grade 1008) and the permanent magnet (NdFeB, Grade N45) are performed. The CAD-model, used for the simulations, is shown in Fig. 1. Based on the illustrated coordinate system, the mover torque around the x-axis is evaluated in relation to

the angular deflection  $\alpha$  and the coil current  $i_{coil}$ . The resulting torque is shown in Eq. (4), marked by circles.

The torque determined by the magnetic equivalent circuit model in Eq. (4), is evaluated in a range of  $\pm 4^\circ$  and an coil current in range of  $\pm 1$  A, as shown in Fig. 3 with solid lines. Since  $R_s$  is a parasitic stray reluctance and the yoke reluctance  $R_y$  is non-linearly and locally depending on the operating point, these parameters are evaluated by FEM simulations. The remaining parameters are adopted according to the model used in the FEM simulations. As expected from the state of the art, the non-linear system behavior of conventional HRAs is observable in the simulation and the model results [20, 21].

This non-linear behaviour is majorly caused by the following two effects. Firstly, the deflection gradient of the mover torque is changing due to the unequal distribution of the permanent magnet flux  $\Phi_m$  in the parallel connected reluctances  $R_1(\alpha)$  and  $R_2(\alpha)$  for  $\alpha \neq 0$ . Secondly, the current to torque relation is increasing towards the mover deflection limits, observable by the increasing torque change for the equidistantly distributed coil currents towards higher deflections, since the stray reluctance  $R_s$  is connected in parallel to the reluctances  $R_1(\alpha)$  and  $R_2(\alpha)$ . E.g for  $\alpha = 0$ , the permanent magnet flux  $\Phi_m$  is distributed between  $R_1(\alpha)$ ,  $R_2(\alpha)$  and  $R_s$ , but towards the mover deflection limits, either  $R_1(\alpha)$  or  $R_2(\alpha)$  becomes relatively small in comparison to  $R_s$ , and the main flux path of the permanent magnet is either  $R_1(\alpha)$  or  $R_2(\alpha)$ . An example of a low stray flux HRA from [25] confirms that behavior. However, the problem with the unequal distribution of the permanent magnet flux  $\Phi_m$  in the parallel connected reluctances  $R_1(\alpha)$  and  $R_2(\alpha)$  is still present. Beyond that, the simulation results are in good agreement with the introduced model to describe the behaviour of a rotational HRA in range of  $\pm 3^\circ$ . Minor model errors occur towards larger angular deflections, originating from the unmodelled saturation effects of the ferromagnetic parts and the small angle approximation, as well as the non-uniform air gap length of the reluctances  $R_1(\alpha)$  and  $R_2(\alpha)$ . To avoid major saturation effects of the ferromagnetic parts, the cross-sections are designed to be sufficiently large. Despite these model errors, the magnetic equivalent circuit model achieves an RMS error of 10.32 mN m compared to the FEM simulation results in full range. The introduced model shows sufficient accuracy and simplicity to apply the subsequent hardware linearization of HRAs to reduce the non-linear effects of the unequally distributed permanent magnet flux and the stray reluctance induced non-linearity.

### 3. Hardware linearization of HRAs

Based on the verified model, a design method to improve the linearity of the conventional HRA is analytically derived. The analytical results of the introduced design approach are evaluated using FEM simulations and compared to the magnetic equivalent circuit model.

The goal of the hardware linearization is a linear HRA with the mover torque described by

$$\tau_{lin} = k_m i_{coil} + \kappa \alpha \quad (5)$$

iii

with the rotational stiffness  $\kappa$  and the motor constant  $k_m$ , which are defined by

$$\begin{aligned} \kappa &= \frac{d\tau}{d\alpha}, \\ k_m &= \frac{d\tau}{di_{coil}}. \end{aligned} \quad (6)$$

These first order derivatives of the mover torque  $\tau$  must be non-zero, otherwise the HRA design is not valid. For instance, if the motor constant  $k_m$  is zero, the torque is independent of the coil current, losing the required connection of the electrical and the mechanical domain in an electromechanical actuator. The targeted model, defined in Eq. (5), implies a linear system behaviour, requiring the higher order derivatives to be zero

$$\begin{aligned} \frac{d^n \tau}{d\alpha^n} &\stackrel{!}{=} 0 \quad \text{with } n \in \mathbb{N}, \quad n \geq 2 \\ \frac{d^n \tau}{di_{coil}^n} &\stackrel{!}{=} 0. \end{aligned} \quad (7)$$

By applying Eq. (7) on the mover torque of the conventional HRA, defined in Eq. (4), the previously discussed non-linearity is observable as non-zero higher order derivatives. Closer investigations showed that higher order derivatives with respect to current are zero for the operating point of  $\alpha = 0^\circ$ , which is visible in Fig. 3 by the equally distributed torque for variable coil currents of  $\pm 1$  A. Consequently, conventional HRAs can be linearly approximated in a sufficiently small range, justifying the claimed linearization of the actuation torque or force by the biasing flux of the permanent magnet [12, 13, 17, 5, 20]. However, large range applications require linearity in full range.

The underlying idea of the hardware linearization is to adapt the mechanical structure to obtain a linear system behavior in a fundamentally non-linear system, as shown for various sensors in [44]. Since, the parasitic stray reluctances  $R_s$  can hardly be chosen in a HRA design and the reluctances of the yoke  $R_y$ , the air gap above the permanent magnet  $R_g$  and the permanent magnet  $R_m$  are independent of the mover deflection, only the reluctances of the working air gaps  $R_1(\alpha)$ ,  $R_2(\alpha)$  are used as design degrees of freedom for the hardware linearization.

To model the mover torque with the general mover deflection-dependent reluctances of  $R_1(\alpha)$ ,  $R_2(\alpha)$ , Eq. (4) needs to be extended due to the potentially variable cross-sections of the working air gaps. The generalized torque of a HRA with variable cross-sections  $A_1(\alpha)$  and  $A_2(\alpha)$  of the working air gaps is

$$\tau_{gen}(\alpha, i_{coil}) = \frac{\Phi_m^2(\alpha, i_{coil})}{2\mu_0 A_1(\alpha)} y_s - \frac{\Phi_m^2(\alpha, i_{coil})}{2\mu_0 A_2(\alpha)} y_s. \quad (8)$$

By solving the differential equations, defined in Eq. (7), with the generalized torque (8) for the generalized reluctances  $R_1(\alpha)$ ,  $R_2(\alpha)$ , no valid solution is found. This might be an indication, that the reluctances of the working air gaps  $R_1(\alpha)$ ,  $R_2(\alpha)$  can not be adapted, such that the mover torque is linearly dependent on the mover deflection  $\alpha$  and the coil current  $i_{coil}$ . Since, there are no further deflection-dependent reluctances available for the hardware linearization, the model complexity is reduced

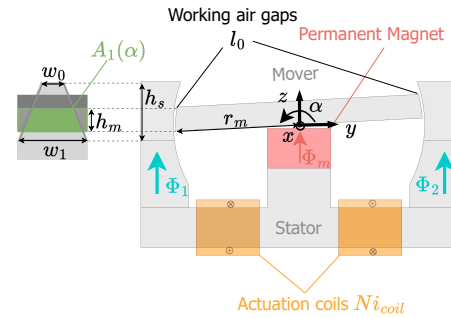


Figure 4: Solution I: Linearized HRA with linear cross-section dependency  $A_{1,2}(\alpha)$  of the working reluctance  $R_{1,2}(\alpha)$ , realized by the trapezoidal stator cross-section. The mover is rotational symmetric around the x-axis to keep both the air gap lengths constant to  $l_0$ .

by neglecting the yoke reluctances  $R_y$  for the following investigations. By limiting the mover deflection to its initial position  $\alpha = 0^\circ$  for the torque derivatives with respect to the coil current and by limiting the coil current  $i_{coil} = 0$  A for the torque derivatives with respect to the mover deflection, two solutions with the generalized reluctances

$$\begin{aligned} R_1(\alpha) &= \frac{L_1(\alpha)}{\mu_0 A_1(\alpha)} \\ R_2(\alpha) &= \frac{L_2(\alpha)}{\mu_0 A_2(\alpha)} \end{aligned}$$

with

$$\begin{aligned} \text{I: } L_{1,2}(\alpha) &= l_0 & \text{or II: } L_{1,2}(\alpha) &= \frac{1}{l_0 \mp l_1 \alpha} \\ A_{1,2}(\alpha) &= a_0 \mp a_1 \alpha & A_{1,2}(\alpha) &= a_0 \end{aligned} \quad (9)$$

with the variable cross-sections  $A_{1,2}(\alpha)$  and the variable air gap lengths  $L_{1,2}(\alpha)$  are identified. In contrast to the conventional HRA, the rotational stiffness  $\kappa$  remains constant for no coil current and the motor constant  $k_m$  is constant at the initial mover deflection with both solutions, representing an fundamental enhancement. Further analytical investigations without the limitation of the mover deflection and the coil current revealed, that the torque derivatives higher order than three ( $n > 3$  in Eq. (7)) are zero for both solutions. For comparison, the torque derivatives of the conventional HRA up to order  $n = 100$  are identified to be non-zero. Based on the reduced number of the non-zero torque derivatives for both solutions, a significantly improved linearity in the entire operating range is expected in relation to the conventional HRA design.

In the following subsections, two exemplary linear HRA designs, which implement the solutions I, II of the reluctances  $R_{1,2}$ . The remaining components, such as the permanent magnet or the actuation coils, are adopted from the conventional HRA to ensure an reasonable performance overview of each HRA design. Both hardware linearized HRA designs are evaluated with respect to linearity by FEM simulations.

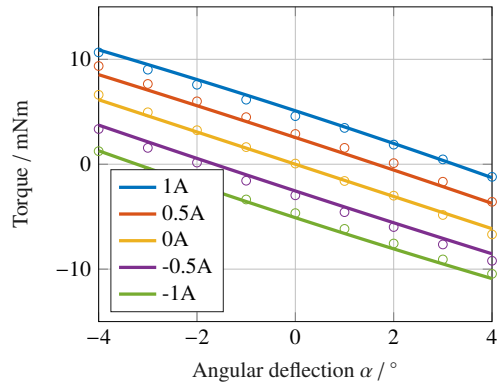


Figure 5: Mover torque of the linearized HRA with linear cross-section dependency  $A_{1,2}(\alpha)$ : Solution I. Comparison of the FEM simulations (circles) and the magnetic equivalent circuit (lines) at various coil currents  $i_{coil}$ , indicating improved linearity in comparison to the conventional HRA.

### 3.1. Solution I: Linear cross-section

Solution I in Eq. (9) requires reluctances  $R_{1,2}(\alpha)$  with linearly increasing and decreasing cross-sections  $A_{1,2}(\alpha)$  and constant air gap lengths  $l_0$  of the working air gaps. To design a structure with the mentioned characteristics, two design steps are essential. Firstly, to keep the air gap length constant  $l_0$ , the mover surface, as well as the stator surface at the working air gaps, are rotationally symmetrical designed around the x-axis with the radius  $r_m$ , as visible in Fig. 4.

Secondly, to obtain a linearly increasing cross-section  $A_{1,2}(\alpha)$ , the mover has a rectangular cross-section in the xz-plane while the stator has a trapezoidal shape, as shown in Fig. 4. The effective cross-section of the air gap is equivalent to the convolution of the rectangular mover cross-section  $A_m$  and the trapezoidal stator cross-section  $A_s$ :

$$A_1(\alpha) = \int_{\gamma_{min}}^{\gamma_{max}} A_s(\gamma) A_m(\alpha - \gamma) d\gamma$$

$$= \underbrace{-\frac{w_0 - w_1}{h_s} h_m \alpha}_{a_1} + \underbrace{h_m w_0 + \frac{w_1 - w_0}{2h_s} h_m^2}_{a_0} \quad (10)$$

with the geometric parameters  $w_0, w_1, h_s, h_m$ , defined in Fig. 4. By comparing the coefficients of Eq. (9) and Eq. (10), the geometric parameters can be related to the gradient of the variable cross-section  $a_1$  and the cross-section of the initial mover position  $a_0$ .

These design steps lead to the linearized HRA design, shown in Fig. 4. Based on the introduced design, FEM simulations are used to evaluate the mover torque. Since the stray reluctance  $R_s$  is a parasitic phenomenon and the magnetic field is not exactly homogeneous in the air gaps, the parameters  $a_1, a_0$ , as well as  $R_s$  are also evaluated by a least-squares fit of magnetic equivalent circuit model to the FEM simulations. However, the comparison of the parameters  $a_1$  and  $a_0$  expressed in Eq. (10) and the simulations are within the same order of magnitude.

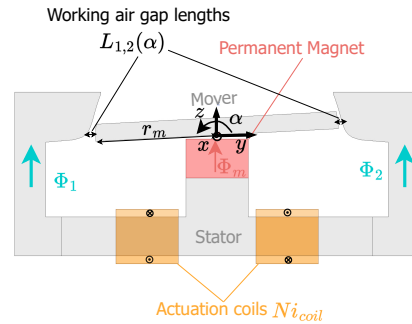


Figure 6: Solution II: Linearized HRA with hyperbolic air gap length dependency  $L_{1,2}(\alpha)$  of the working reluctance  $R_{1,2}(\alpha)$ , realized by the parameterized shape of the stator surface facing towards the mover. The mover is rotational symmetric around the x-axis with the radius  $r_m$ .

The modeled and simulated mover torques over an angular range of  $\pm 4^\circ$  and an coil current in range of  $\pm 1$  A are compared in Fig. 5 with solid lines and circles, respectively. An improved linearity is clearly observable compared to the conventional HRA torque, shown in Fig. 3. A minor non-linearity shows up toward increasing coil currents for angular deflections close to the maximum range of  $\pm 4^\circ$ . This non-linearity is expected to be present, as the proposed hardware linearization is only analytically exact for either  $i_{coil} = 0$  A or  $\alpha = 0^\circ$  and non-zero torque derivatives are identified up to the order of three.

By fitting a linear model from Eq. (5), to the simulated torque, a motor constant of  $k_m = 4.98$  mNm A $^{-1}$  and a rotational stiffness of  $\kappa = 87.6$  mNm rad $^{-1}$  are determined. The fitted linear model shows a RMS error of 0.432 mNm, which is highly linear compared to conventional HRAs with a linearity error of 27.7 mNm.

A limitation of this linearly dependent cross-section design is its relatively low motor constant. This limitation arises due to the constrained gradient of the cross-section  $a_1$ , which is influenced by geometric parameters such as  $w_0, w_1, h_s$ , and  $h_m$ . These constraints originate from the need for compact size in HRAs, thereby it is undesired to increase the width  $w_1$  or the stator height  $h_s$ . Also the minimum mover height  $h_m$  is limited, since the mover needs to be sufficiently rigid to withstand the acting torques. Furthermore, saturation effects of the ferromagnetic parts limit the smallest cross-section, defined by the width  $w_0$  paired with the mover height  $h_m$ . Summing up, this design improves the linearity by a factor of 64, but decreases the motor constant by 81 % compared to conventional HRAs.

### 3.2. Solution II: Hyperbole air gap length

Solution II in Eq. (9) requires reluctances  $R_{1,2}(\alpha)$  with hyperbolically increasing and decreasing air gap lengths  $L_{1,2}(\alpha)$  and constant cross-sections  $a_0$  of the working air gaps. To design a structure with the desired behavior, the following adaptations of the conventional HRA are made.

The mover cross-section is selected to be constant and rectangular in the xz-plane. The mover surfaces at the working air

gaps are rotationally symmetrical around the x-axis with the radius  $r_m$ , as visible in Fig. 4. To obtain a hyperbolically increasing and decreasing air gap length  $L_{1,2}(\alpha)$ , the stator surface facing the mover is parameterized by

$$\begin{aligned} y_{1,2}(\alpha) &= (r_m + L_{1,2}(\alpha)) \cos \alpha \\ z_{1,2}(\alpha) &= (r_m + L_{1,2}(\alpha)) \sin \alpha \end{aligned} \quad (11)$$

in the  $yz$ -plane, as illustrated in Fig. 6. Since the mover rotates around the x-axis, the air gap length  $L_{1,2}(\alpha)$  is added to the mover radius  $r_m$ , ensuring a hyperbolic variation in the air gap length with respect to the angular deflection  $\alpha$ .

Based on the introduced HRA design, FEM simulations are used to evaluate the mover torque. The parasitic stray reluctance  $R_s$  is calibrated by finite simulative analysis, in accordance to the conventional and the solution I HRA design. Since the magnetic field is not exactly homogeneous in the working air gaps and the effective length is influenced by the height of the mover  $h_m$ , the parameters  $l_0$  and  $l_1$  of the parameterized air gap length  $L_{1,2}(\alpha)$  are also determined by a least-squares fit of the magnetic equivalent model to the FEM simulations. However, the comparison of the parameters  $l_1$  and  $l_0$  expressed in Eq. (11) and the simulations are within the same order of magnitude. As discussed previously, the target of this study is to find a structure with a hyperbolic increasing/decreasing air gap length. The remaining parameters, such as the coercivity of the permanent magnet  $H_c$ , the corresponding permanent magnet length  $l_m$  or the number of turns  $N$  are adopted from the conventional and the solution I HRA design.

Finally, the mover torques modeled and simulated in an angular range of  $\pm 4^\circ$  and an coil current in a range of  $\pm 1$  A are compared in Fig. 7 with solid lines and circles, respectively. An improved linearity is observable compared to the conventional HRA torque, shown in Fig. 3. Especially, the linearity for  $\alpha = 0^\circ$  with respect to the current to torque relation and the linearity for  $i_{coil} = 0$  A regarding the angular deflection to torque relation. This effect corresponds to the previously defined condition of limiting the operating points to find a solution for the differential equations (7), verifying the approach of the analytical hardware linearization. A minor non-linearity is observable towards increasing coil currents for angular deflection close to the limits of  $\pm 4^\circ$ , which is expected, since non-zero torque derivatives up to the order of three are analytically determined in the entire range of the HRA.

By fitting the linear model, defined in Eq. (5), to the simulated torque, an improved motor constant by factor 2 of  $k_m = 9.59 \text{ mN m A}^{-1}$  is obtained compared to the solution I and a rotational stiffness of  $\kappa = 97.0 \text{ mN m rad}^{-1}$  is determined for the HRA design of the solution II. With an RMS error of  $0.580 \text{ mN m}$ , the linearity is significantly increased compared to the conventional HRA of  $27.7 \text{ mN m}$ .

However, considering the saturation effects of the ferromagnetic material, this design also has its limitations with respect to the motor constant. A higher motor constant is achieved by increasing the gradient of the working reluctances  $R_{1,2}(\alpha)$  [45]. By increasing the gradient of the working reluctances, the air gap length decreases at the maximum angular deflection. With

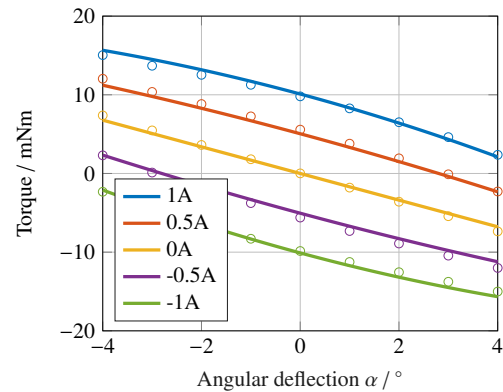


Figure 7: Mover torque of the linearized HRA with hyperbolic air gap length dependency  $L_{1,2}(\alpha)$ ; Solution II. Comparison of the FEM simulations (circles) and the magnetic equivalent circuit (lines) at various coil currents  $i_{coil}$ , indicating improved linearity in comparison to the conventional HRA.

an unchanged MMF of the permanent magnet and the actuation coils, the flux is increased at maximum angular deflection, which is limited by the saturation effects of the ferromagnetic material. Apart from that, the mover height  $h_m$  could be decreased to reduce the averaging effect of the air gap length, but to avoid saturation effects the mover width in x-direction needs to be accordingly increased. By increasing the mover width, the desirable compactness of the actuator is reduced, as well as the mechanical stiffness of the mover against the actuator torque is reduced. Therefore, the geometry of the working air gaps  $R_{1,2}$  is tuned, considering the trade-off of on the one hand, to stay within the saturation boundaries of the ferromagnetic material with a mover width of 9 mm and on the other hand to obtain a reasonable motor constant.

#### 4. Linearized HRAs vs. conventional HRA

The reasonable selection of the proposed linearized HRA designs or the conventional HRA depends greatly on the final application and the desired system specifications. As this paper is especially interested in the linearity of HRAs for high precision applications and the main task of a rotational electromagnetic actuator is to obtain high output torques of low currents for high efficiency, a performance comparison between these two parameters is provided in Fig. 8.

The linearity error of each design is defined by the RMS error of the fitted linear model from Eq. (5). Since fast steering mirrors are operated predominantly around the initial position of  $\alpha \approx 0^\circ$  in scanning applications, the motor constant is evaluated at this operating point. The linearized HRA design with the hyperbolic air gap length dependency, as well as the design with the linear cross-section dependency, significantly improves the linearity in comparison to the conventional HRA, as observable in Fig. 8. The linearity error could be reduced from  $27.7 \text{ mN m}$  to  $0.432 \text{ mN m}$  (solution I) and  $0.580 \text{ mN m}$  (solution II), resulting in an improvement by a factor of 50.

The motor constant of the better performing linearized HRA design is reduced by a factor of 2.7 compared to the conventional HRA. As the angular deflection gradient of the working reluctances  $R_{1,2}(\alpha)$  of the linearized HRAs are smaller in comparison to the conventional HRA design, a decreased motor-constant is expected. This indicates a trade-off between linearity and motor constant. Considering application requiring highest energy efficiency, the optimization of the current to torque relation, e.g. by topology optimization [46], and a non-linear control approach [34] could be more efficient. Whereas, for resonant fast steering mirrors, the linearized HRA approach could be more efficient, since the resonance is not shifted in contrast to conventional HRAs [22]. Due to the highly linear behavior of Lorentz actuators, or more specifically voice coil actuators, they are commonly used in high-precision applications. With respect to them, conventional HRAs obtain an up to 9.6 improved motor constant [2], i.e. the introduced linearized HRAs have an up to factor 3.5 higher motor-constant than voice coil actuators, as observable in Fig. 8. Additionally, conventional HRAs show a higher range-bandwidth-product in comparison to Lorentz actuators in high performance mechatronic systems [1]. Therefore, the proposed linearized HRA designs might be able to enhance the performance of mechatronic systems, being a reasonable actuator choice to outperform Lorentz actuated high-precision systems.

### 5. Tip/tilt fast steering mirror

For the targeted utilization in fast steering mirrors, an extension by a second axis is required for many applications [17, 1]. The second axis can be implemented by another decoupled magnetic circuit in a serial kinematic approach, which is equivalent to the proposed linearized HRA approaches. The decoupled design ensures the system linearity and avoids the non-linearity, originating from the permanent magnet flux distribution in the working air gaps and the stray reluctance effects, as shown for the one-degree-of-freedom linearized HRA. With regard to the compactness of tip/tilt fast steering mirrors, a coupled magnetic circuit with only one permanent magnet in the center for both axes would be reasonable with a parallel kinematic approach, as introduced in [21, 20]. However, the additional reluctances for the second axis impair the distribution of the permanent magnet flux, expecting a cross-talk between the tip/tilt axis. Additionally, a tilt of the second axis changes the reluctances in the tip axis. Therefore, further work towards linear tip/tilt fast steering mirrors is required and their experimental validation.

In summary, the air gap shaping approach to improve linearity resulted in two HRA designs, one with linear cross-section dependency and the other with hyperbolic air gap length dependency. Both designs improve linearity by a factor of 50 in comparison to conventional HRAs and provide a higher motor constant than Lorentz actuators.

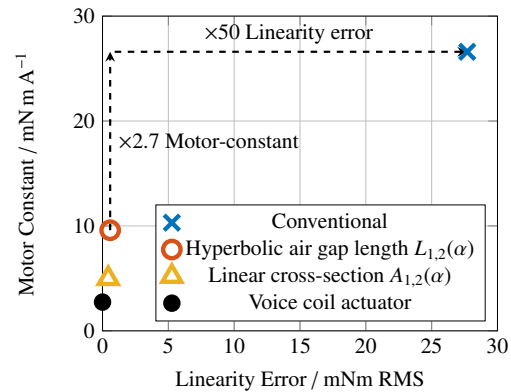


Figure 8: Performance comparison of the introduced linearized HRAs, the conventional HRA and an ideally linear voice coil actuator with the relative motor-constant from [2]. The linearized HRAs indicate an improved linearity, but reduced motor-constants, in comparison to the conventional HRA. With respect to the motor-constant of voice coil actuators, the linearized HRAs outperform them significantly.

### 6. Conclusion

This paper presents an air gap shaping approach to improve the linearity of rotational HRAs used in fast steering mirrors. The approach involves modeling a one-degree-of-freedom HRA, using a magnetic equivalent circuit to identify and analyze sources of the non-linear system behavior. The non-linear behavior of conventional HRAs is observable in the mover torque with respect to the angular deflection and coil current.

Based on the verified magnetic equivalent circuit, differential equations are derived to enhance linearity. Two linearized HRA designs are proposed, one with a linear cross-section dependency and the other with a hyperbolic air gap length dependency. FEM simulations are employed to evaluate the performance with respect to the linearity and the motor constant of these designs. The proposed hardware linearized HRAs show a substantial improvement in the linearity error, reducing it by a factor of 50 compared to conventional HRA designs. The results clearly indicate a trade-off between the motor constant and the linearity. The linearized HRA designs show a reduced motor constant, but offer significantly enhanced linearity. Compared to Lorentz actuators, the linearized HRAs offer better performance with respect to the motor constant, these actuator designs are potential candidates for high-precision applications to further enhance mechatronic systems. Future investigations could further develop the linearization by air gap designs applicable to magnetically coupled tip/tilt fast steering mirrors.

### Acknowledgement

This work was supported by Micro-Epsilon Messtechnik GmbH and Co. KG.

## References

- [1] E. Csencsics, G. Schitter, Exploring the pareto fronts of actuation technologies for high performance mechatronic systems, *IEEE/ASME Transactions on Mechatronics* 26 (2) (2021) 1053–1063. doi:10.1109/tmech.2020.3016087.
- [2] F. Cigarini, S. Ito, S. Troppmair, G. Schitter, Comparative finite element analysis of a voice coil actuator and a hybrid reluctance actuator, *IEEE Journal of Industry Applications* 8 (2) (2019) 192–199. doi:10.1541/ieejia.8.192.
- [3] X. Zhang, L. Lai, L. Zhang, L. Zhu, Hysteresis and magnetic flux leakage of long stroke micro/nanopositioning electromagnetic actuator based on maxwell normal stress, *Precision Engineering* 75 (2022) 1–11. doi:10.1016/j.precisioneng.2022.01.003.
- [4] L. Chen, Y. Niu, X. Yang, W.-L. Zhu, L.-M. Zhu, Z. Zhu, A novel compliant nanopositioning stage driven by a normal-stressed electromagnetic actuator, *IEEE Transactions on Automation Science and Engineering* 19 (4) (2022) 3039–3048. doi:10.1109/tase.2021.3105683.
- [5] S. Ito, S. Troppmair, B. Lindner, F. Cigarini, G. Schitter, Long-range fast nanopositioner using nonlinearities of hybrid reluctance actuator for energy efficiency, *IEEE Transactions on Industrial Electronics* 66 (4) (2019) 3051–3059. doi:10.1109/tie.2018.2842735.
- [6] X. Du, D. Shen, P. Huang, L. Zhu, Z. Zhu, Dual-stage fast tool servo cascading a primary normal-stressed electromagnetic stage with a secondary piezo-actuated stage, *Precision Engineering* 80 (2023) 171–179. doi:10.1016/j.precisioneng.2022.12.005.
- [7] S. Ito, B. Lindner, G. Schitter, Sample-tracking vibration isolation with hybrid reluctance actuators for inline metrology, *IFAC-PapersOnLine* 52 (15) (2019) 537–542. doi:10.1016/j.ifacol.2019.11.731.
- [8] S. Ito, F. Cigarini, G. Schitter, Flux-controlled hybrid reluctance actuator for high-precision scanning motion, *IEEE Transactions on Industrial Electronics* 67 (11) (2020) 9593–9600. doi:10.1109/tie.2019.2952829.
- [9] G. Stadler, E. Csencsics, S. Ito, G. Schitter, High precision hybrid reluctance actuator with integrated orientation independent zero power gravity compensation, *IEEE Transactions on Industrial Electronics* 69 (12) (2022) 13296–13304. doi:10.1109/tie.2021.3137444.
- [10] R. Bowens-Rubin, P. Hinz, S. Kuiper, D. Dillon, Performance of large-format deformable mirrors constructed with hybrid variable reluctance actuators ii: initial lab results from flash, in: S. B. Shaklan, G. J. Ruane (Eds.), *Techniques and Instrumentation for Detection of Exoplanets X*, SPIE, 2021. doi:10.1117/12.2593535.
- [11] R. Bowens-Rubin, P. M. Hinz, W. Jonker, S. Kuiper, C. Laguna, M. Maniscalco, Performance of large-format deformable mirrors constructed with two variable reluctance actuators, in: D. Schmidt, L. Schreiber, E. Vernet (Eds.), *Adaptive Optics Systems VII*, SPIE, 2020. doi:10.1117/12.2563659.
- [12] D. Wu, X. Xie, S. Zhou, Design of a normal stress electromagnetic fast linear actuator, *IEEE Transactions on Magnetics* 46 (4) (2010) 1007–1014. doi:10.1109/tmag.2009.2036606.
- [13] X.-D. Lu, D. Trumper, Ultrafast tool servos for diamond turning, *CIRP Annals* 54 (1) (2005) 383–388. doi:10.1016/s0007-8506(07)60128-0.
- [14] W.-W. Huang, Z. Zhu, X. Zhang, L.-M. Zhu, A hybrid electromagnetic-piezoelectric actuated tri-axial fast tool servo integrated with a three-dimensional elliptical vibration generator, *Precision Engineering* 86 (2024) 213–224. doi:10.1016/j.precisioneng.2023.12.006.
- [15] P. Immonen, V. Ruuskanen, J. Pyrhönen, Moving magnet linear actuator with self-holding functionality, *IET Electrical Systems in Transportation* 8 (3) (2018) 182–187. doi:10.1049/iet-est.2017.0079.
- [16] D. Kluk, M. Boulet, D. L. Trumper, A high-bandwidth, high-precision, two-axis steering mirror with moving iron actuator, *IFAC Proceedings Volumes* 43 (18) (2010) 552–557. doi:10.3182/20100913-3-us-2015.00133.
- [17] D. J. Kluk, M. T. Boulet, D. L. Trumper, A high-bandwidth, high-precision, two-axis steering mirror with moving iron actuator, *Mechatronics* 22 (3) (2012) 257–270. doi:10.1016/j.mechatronics.2012.01.008.
- [18] S. Kuiper, W. Crowcombe, J. Human, B. Dekker, E. Nieuwkoop, A. Meskers, Gert, High-bandwidth and compact fine steering mirror development for laser communications, *Tech. Rep. the* (2017).
- [19] F. Claeysen, K. Benoit, G. Aigouy, T. Maillard, M. Fournier, O. Sosnicki, Large stroke fast steering mirror for space free-space optical communication, 2020.
- [20] E. Csencsics, J. Schlarp, T. Schopf, G. Schitter, Compact high performance hybrid reluctance actuated fast steering mirror system, *Mechatronics* 62 (2019) 102251. doi:10.1016/j.mechatronics.2019.102251.
- [21] E. Csencsics, J. Schlarp, G. Schitter, High-performance hybrid-reluctance-force-based tip/tilt system: Design, control, and evaluation, *IEEE/ASME Transactions on Mechatronics* 23 (5) (2018) 2494–2502. doi:10.1109/tmech.2018.2866272.
- [22] J. Schlarp, E. Csencsics, G. Doblinger, G. Schitter, Design of a mechanical tunable resonant fast steering mirror, in: 2020 IEEE/ASME International Conference on Advanced Intelligent Mechatronics (AIM), Boston, USA (Virtual Conference), July 6–9, 2020, IEEE, 2020.
- [23] Y. Long, J. Mo, X. Wei, C. Wang, S. Wang, Design of a moving-magnet electromagnetic actuator for fast steering mirror through finite element simulation method, *Journal of Magnetics* 19 (3) (2014) 300–308. doi:10.4283/jmag.2014.19.3.300.
- [24] Y. Long, J. Mo, X. Chen, Q. Liang, Y. Shang, S. Wang, Design of a rotary electromagnetic actuator with linear torque output for fast steering mirror, in: *Journal of Magnetics*, Vol. 20, 2015, pp. 69–78. doi:http://dx.doi.org/10.4283/JMAG.2015.20.1.069.
- [25] W. Zhang, W. Li, X. Zheng, W. Yu, H. Huang, Modeling and designing a hybrid reluctance actuator for fast-steering mirror, Vol. 61. *SPIE-Intl Soc Optical Eng.* 2022. doi:10.1117/1.OE.61.5.054106.
- [26] H. F. Mokbel, W. Yuan, L. Q. Ying, C. G. Hua, A. A. Roshdy, Research on the mechanical design of two-axis fast steering mirror for optical beam guidance, in: *Proceedings of the 1st International Conference on Mechanical Engineering and Material Science*, Atlantis Press, 2012. doi:10.2991/mems.2012.137.
- [27] M. Guelman, A. Kogan, A. Kazarian, A. Livne, M. Orenstein, H. Michalik, S. Arnon, Acquisition and pointing control for inter-satellite laser communications, *IEEE Transactions on Aerospace and Electronic Systems* 40 (4) (2004) 1239–1248. doi:10.1109/taes.2004.1386877.
- [28] S. Xiang, P. Wang, S. Chen, X. Wu, D. Xiao, X. Zheng, The research of a novel single mirror 2d laser scanner, in: *SPIE Proceedings*, Vol. 7382, 2009, p. 73821A. doi:10.1117/12.832651.
- [29] M. Hafez, T. Sidler, R. Salathé, G. Jansen, J. Compter, Design, simulations and experimental investigations of a compact single mirror tip/tilt laser scanner, *Mechatronics* 10 (7) (2000) 741–760. doi:10.1016/s0957-4158(99)00093-8.
- [30] L. R. Hedding, R. A. Lewis, Fast steering mirror design and performance for stabilization and single-axis scanning, in: *SPIE Proceedings*, 1990, pp. 14–24. doi:10.1117/12.21547.
- [31] Q. Zhou, P. Ben-Tzvi, D. Fan, A. A. Goldenberg, Design of fast steering mirror systems for precision laser beams steering, in: 2008 International Workshop on Robotic and Sensors Environments, IEEE, 2008. doi:10.1109/rose.2008.4669196.
- [32] H. W. Yoo, M. E. van Royen, W. A. van Cappellen, A. B. Houtsmuller, M. Verhaegen, G. Schitter, Automated spherical aberration correction in scanning confocal microscopy, *Review of Scientific Instruments* 85 (12) (2014). doi:10.1063/1.4904370.
- [33] D. Wertjan, E. Csencsics, T. Kern, G. Schitter, Bringing the lab to the fab: Robot-based inline measurement system for precise 3-d surface inspection in vibrational environments, *IEEE Transactions on Industrial Electronics* 69 (10) (2022) 10666–10673. doi:10.1109/tie.2022.3151959.
- [34] L. Chen, Q. Liu, L. Zhu, Z. Zhu, On the actuation nonlinearity of normal-stressed electromagnetic nanopositioning stages, *Precision Engineering* (2024). doi:10.1016/j.precisioneng.2024.01.009.
- [35] A. Katalenic, J. de Boeij, H. Butler, P. van den Bosch, Linearization of a current-driven reluctance actuator with hysteresis compensation, *Mechatronics* 23 (2) (2013) 163–171. doi:10.1016/j.mechatronics.2013.01.004.
- [36] T. Zhu, B. Cazzolato, W. S. Robertson, A. Zander, Vibration isolation using six degree-of-freedom quasi-zero stiffness magnetic levitation, *Journal of Sound and Vibration* 358 (2015) 48–73. doi:10.1016/j.jsv.2015.07.013.
- [37] J. Lindlau, C. Knospe, Feedback linearization of an active magnetic bearing with voltage control, *IEEE Transactions on Control Systems Technol-*

- ogy 10 (1) (2002) 21–31. doi:10.1109/87.974335.
- [38] D. Trumper, S. Olson, P. Subrahmanyam, Linearizing control of magnetic suspension systems, *IEEE Transactions on Control Systems Technology* 5 (4) (1997) 427–438. doi:10.1109/87.595924.
- [39] C.-T. Hsu, S.-L. Chen, Exact linearization of a voltage-controlled 3-pole active magnetic bearing system, *IEEE Transactions on Control Systems Technology* 10 (4) (2002) 618–625. doi:10.1109/tcst.2002.1014681.
- [40] L. Li, Linearizing magnetic bearing actuators by constant current sum, constant voltage sum, and constant flux sum, *IEEE Transactions on Magnetics* 35 (1) (1999) 528–535. doi:10.1109/20.737477.
- [41] G. Forstner, A. Kugi, W. Kemmetmüller, A magnetic equivalent circuit based modeling framework for electric motors applied to a pmsm with winding short circuit, *IEEE Transactions on Power Electronics* 35 (11) (2020) 12285–12295.
- [42] W. Zhang, J. Yuan, C. Yan, Z. Gao, Y. Dong, Multi-objective optimization design of natural frequency of two-degree-of-freedom fast steering mirror system, *IEEE Access* 9 (2021) 33689–33703. doi:10.1109/access.2021.3061473.
- [43] B.-U. Nam, H. Gimm, D. Kang, D. Gweon, Design and analysis of a tip-tilt guide mechanism for the fast steering of a large-scale mirror, *Optical Engineering* 55 (10) (2016) 106120. doi:10.1117/1.oe.55.10.106120.
- [44] T. Islam, S. C. Mukhopadhyay, Linearization of the sensors characteristics: a review, *International Journal on Smart Sensing and Intelligent Systems* 12 (1) (2019) 1–21. doi:10.21307/ijssis-2019-007.
- [45] M. Pumphrey, N. Alatawneh, M. A. Janaideh, Modeling and analysis of reluctance motion system with asymmetrical air gaps, *Review of Scientific Instruments* 93 (7) (2022). doi:10.1063/5.0088120.
- [46] J. S. Choi, J. Yoo, Structural topology optimization of magnetic actuators using genetic algorithms and on/off sensitivity, *IEEE Transactions on Magnetics* 45 (5) (2009) 2276–2279. doi:10.1109/tmag.2009.2016297.



**Georg Schitter** is Professor for Advanced Mechatronic Systems at the Automation and Control Institute (ACIN) of TU Wien. He received an MSc in Electrical Engineering from TU Graz, Austria (2000) and an MSc and PhD degree from ETH Zurich, Switzerland (2004). His primary research interests are on high-performance mechatronic systems, particularly for applications in the high-tech industry, scientific instrumentation, and mechatronic imaging systems, such as AFM, scanning laser and LIDAR systems, telescope systems, adaptive optics, and lithography systems for semiconductor industry. He received the journal best paper award of *IEEE/ASME Transactions on Mechatronics* (2018), of the *IFAC Mechatronics* (2008-2010), of the *Asian Journal of Control* (2004-2005), and the 2013 *IFAC Mechatronics Young Researcher Award*. He served as an Associate Editor for *IFAC Mechatronics*, *Control Engineering Practice*, and for the *IEEE Transactions on Mechatronics*.



**Alexander Pechhacker** is doctoral researcher in the Advanced Mechatronic Systems group at the Automation and Control Institute (ACIN) at TU Wien, Vienna, Austria. He received an MSc degree in Electrical Engineering from TU Wien, Austria in 2022. His primary research interests are on high performance mechatronic systems design, electromagnetic actuator design and high precision position control.



**Ernst Csencsics** is associate professor for Measurement Systems in the Advanced Mechatronic Systems group at the Automation and Control Institute (ACIN) of TU Wien. He received an MSc and a PhD degree (sub auspiciis) in Electrical Engineering from TU Vienna, Austria in 2014 and 2017, respectively. His primary research interests are on high performance mechatronic systems, the development of holistic methods for multidisciplinary system design and integration, opto-mechatronic measurement and imaging systems, precision engineering, and robot-based in-line measurement systems. He received the journal best paper award of *IEEE/ASME Transactions on Mechatronics* (2018) and the best student paper award at the American Control Conference (2016).